The Astrophysical Journal Letters, 816:L11 (6pp), 2016 January 1 doi:10.3847/2041-8205/816/1/L11

ON THE METALLICITY AND ORIGIN OF THE SMITH HIGH-VELOCITY CLOUD*

Andrew J. Fox[1], Nicolas Lehner[2], Felix J. Lockman[3], Bart P. Wakker[4], Alex S. Hill[5], Fabian Heitsch[6], David V. Stark[6,7], Kathleen A. Barger[8], Kenneth R. Sembach[1], and Mubdi Rahman[9]
[1] Space Telescope Science Institute, 3700 San Martin Drive, Baltimore, MD 21218, USA; afox@stsci.edu
[2] Department of Physics, University of Notre Dame, 225 Nieuwland Science Hall, Notre Dame, IN 46556, USA
[3] National Radio Astronomy Observatory, P.O. Box 2, Rt. 28/92, Green Bank, WV 24944, USA
[4] Department of Astronomy, University of Wisconsin–Madison, 475 North Charter St., Madison, WI 53706, USA
[5] Department of Astronomy, Haverford College, 370 Lancaster Ave., Haverford, PA 19041, USA
[6] Department of Physics and Astronomy, University of North Carolina at Chapel Hill, 120 E. Cameron Ave., Chapel Hill, NC 27599, USA
[7] Kavli Institute for the Physics and Mathematics of the universe, 5-1-5 Kashiwanoha, Kashiwa, 277-8583, Japan
[8] Department of Physics and Astronomy, Texas Christian University, TCU Box 298840, Fort Worth, TX 76129, USA
[9] Department of Physics and Astronomy, Johns Hopkins University, 3400 North Charles St., Baltimore, MD 21218, USA
Received 2015 November 20; accepted 2015 December 15; published 2015 December 30

ABSTRACT

The Smith Cloud (SC) is a gaseous high-velocity cloud (HVC) in an advanced state of accretion, only 2.9 kpc below the Galactic plane and due to impact the disk in ≈27 Myr. It is unique among HVCs in having a known distance (12.4 ± 1.3 kpc) and a well-constrained 3D velocity (296 km s^{-1}), but its origin has long remained a mystery. Here we present the first absorption-line measurements of its metallicity, using *Hubble Space Telescope*/COS UV spectra of three active galactic nuclei lying behind the Cloud together with Green Bank Telescope 21 cm spectra of the same directions. Using Voigt-profile fitting of the S II λλ1250, 1253, 1259 triplet together with ionization corrections derived from photoionization modeling, we derive the sulfur abundance in each direction; a weighted average of the three measurements gives [S/H] = −0.28 ± 0.14, or $0.53^{+0.21}_{-0.15}$ solar metallicity. The finding that the SC is metal-enriched lends support to scenarios where it represents recycled Galactic material, rather than the remnant of a dwarf galaxy or accreting intergalactic gas. The metallicity and trajectory of the Cloud are both indicative of an origin in the outer disk. However, its large mass and prograde kinematics remain to be fully explained. If the cloud has accreted cooling gas from the corona during its fountain trajectory, as predicted in recent theoretical work, its current mass would be higher than its launch mass, alleviating the mass concern.

Key words: Galaxy: evolution – Galaxy: halo – ISM: kinematics and dynamics

1. INTRODUCTION

The gaseous halo of the Milky Way is home to a diverse population of high-velocity clouds (HVCs) that do not co-rotate with the underlying disk. HVCs trace a variety of processes including inflow, outflow, tidal stripping, and condensation of coronal material (Wakker & van Woerden 1997). Once the neutral and ionized phases of HVCs are accounted for, they represent a global inflow rate onto the Galaxy of ≈0.4–1.4 $M_\odot$ yr^{-1} (Shull et al. 2009; Lehner & Howk 2011; Putman et al. 2012), similar to the Galactic star-formation rate. HVCs therefore represent the Galactic fuel supply, and understanding their physical and chemical properties allows us to explore the mechanism(s) by which star formation is sustained.

The Smith Cloud (SC; see Figure 1; Smith 1963), also known as the Galactic-Center-Positive (GCP) complex, is a large HVC[10] plunging toward the Galactic plane with a velocity $v_z = 73$ km s^{-1}, a H I mass of $\gtrsim 10^6 M_\odot$ (Lockman et al. 2008), and a similar H II mass (Hill et al. 2009). Its cometary morphology suggests that its direction of motion lies along its major axis, and so its LSR velocity can be used to derive a 3D velocity of 296 km s^{-1} (Lockman et al. 2008), which is lower than the Galactic escape velocity. The SC has a heliocentric distance of $d = 12.4 \pm 1.3$ kpc, based on three independent methods: the detection of absorption lines in background stellar spectra (Wakker et al. 2008), its kinematics (Lockman et al. 2008), and its Hα emission (Putman et al. 2003). It also has a magnetic field of >8 μG detected via Faraday rotation (Hill et al. 2013) but no significant stellar population (Stark et al. 2015). Together, these properties make the SC arguably the best characterized of all HVCs (see Lockman 2015).

Despite the good characterization of the SC's properties, its origin remains unknown. It is unclear whether it represents Galactic material, expelled from the disk as part of a Galactic fountain (Bregman 1980; Spitoni et al. 2008); accreting extragalactic material; the gaseous remnant of a dwarf galaxy, such as the Sagittarius dwarf (Bland-Hawthorn et al. 1998) or other satellite (Stark et al. 2015); or something else. The key missing piece of evidence is the SC metallicity. Metallicity discriminates between recycled Galactic gas (enriched) and infalling extragalactic gas (unenriched), but since the SC lies close to the disk and so has relatively high foreground extinction, there have been (until now) no active galactic nuclei (AGNs) lying behind the SC observed in the UV. Thus there is no published absorption-line constraint on the SC metallicity, though Hill et al. (2009) measured the Hα and [N II] emission from the SC using optical nebular lines and derived a nitrogen abundance of 0.15–0.44 times solar.

* Based on observations taken under program 13840 of the NASA/ESA *Hubble Space Telescope*, obtained at the Space Telescope Science Institute, which is operated by the Association of Universities for Research in Astronomy, Inc., under NASA contract NAS 5-26555, and under program GBT09A_17 of the Robert C. Byrd Green Bank Telescope (GBT) of the National Radio Astronomy Observatory, a facility of the National Science Foundation operated under a cooperative agreement by Associated Universities, Inc.
[10] Parts of the SC are at intermediate velocities $v_{\rm LSR} < 90$ km s^{-1}, but it has traditionally been defined as an HVC since its head is at $v_{\rm LSR} \approx 100$ km s^{-1}.

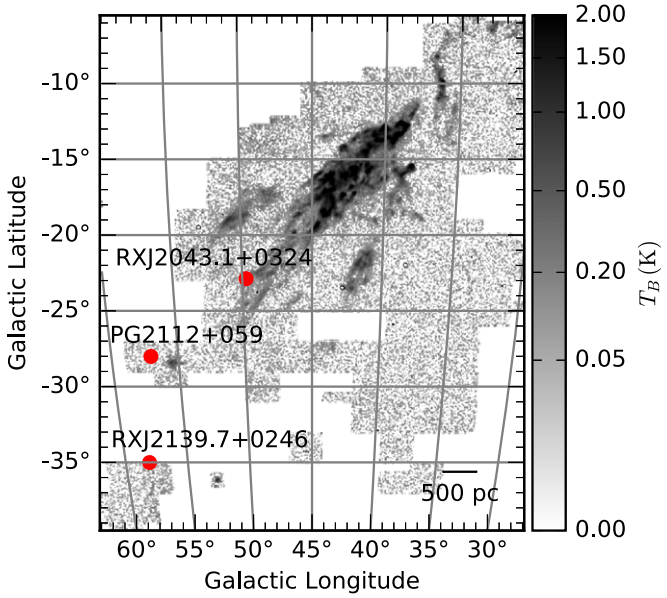

Figure 1. Map of the SC and its surroundings based on Hill et al. (2013). The grayscale shows the brightness temperature of 21 cm H I emission from the Green Bank Telescope at a fixed velocity $v_{\rm GSR} = +247\,{\rm km\,s^{-1}}$ in the Galactocentric standard of rest frame. The three COS targets are shown with red circles. All three probe the major axis of the SC, which is moving toward the upper right in this image, and all three show detections of 21 cm emission from the cloud or its wake.

In this letter we present absorption-line metallicity measurements from three SC sightlines, toward the AGNs PG 2112+059, RX J2043.1+0324, and RX J2139.7+0246. We describe the UV and radio observations in Section 2, present the spectra and abundance calculations in Section 3, and discuss the implications in Section 4. All velocities are presented in the LSR reference frame.

2. OBSERVATIONS AND DATA REDUCTION

The targets for this program were selected by searching for UV-bright AGNs behind or near the SC. This search yielded three targets (see Table 1). All three probe the wake region of the SC, behind its direction of motion (Figure 1), where there is extensive diffuse H I both morphologically and kinematically associated with the cloud (Lockman et al. 2008). The three AGNs were observed in 2014 October with the Cosmic Origins Spectrograph (COS; Green et al. 2012) on board the *Hubble Space Telescope* (*HST*), under Program ID 13840 (PI Fox), with three orbits per target. The spectra were taken with the G130M/1291 grating/central-wavelength combination, the primary science aperture, and all four FP-POS positions. The `x1d` files produced by the `calcos` reduction pipeline were aligned using customized reduction software, designed to ensure that commonly observed ISM lines are aligned in wavelength space (see Wakker et al. 2015 for more details). The data were binned by three pixels and continuum normalized for display.

H I 21 cm spectra were taken with the 100 m Robert C. Byrd Green Bank Telescope (GBT) at an angular resolution of 9.′1, under project code GBT09A_17. Spectra were taken using in-band frequency switching, and covered 700 km s^{-1} centered at zero velocity LSR at a velocity resolution of 1.3 km s^{-1}. The data were calibrated and corrected for stray radiation following the procedure described in Boothroyd et al. (2011), and a low-order polynomial was fit to emission-free regions of the spectra to remove residual instrumental baseline structure. The H I column density in each direction is calculated by integrating the 21 cm brightness-temperature profiles (shown in Figure 2) between $v_{\rm min}$ and $v_{\rm max}$ by the standard relation

$$N({\rm H\,I}) = 1.823 \times 10^{18}\,{\rm cm^{-2}} \int_{v_{\rm min}}^{v_{\rm max}} T_B\,{\rm d}v. \quad (1)$$

For the PG 2112+059 direction, the SC component is blended on the blue (low-velocity) side by Galactic emission, so in this case we determined the H I column density by fitting a Gaussian component, with a velocity centroid matching that seen in S II absorption.

3. RESULTS

Among the many low-ionization lines in the COS G130M bandpass, the S II $\lambda\lambda$1250, 1253, 1259, and O I λ1302 lines are the most useful for metallicity measurements, because sulfur and oxygen are relatively undepleted onto dust and have relatively small ionization corrections (ICs). Unfortunately, the O I λ1302 lines from the SC are of very limited use for metallicity measurements because of strong saturation. This leaves the S II triplet as our best metallicity indicator. *HST*/COS absorption-line profiles showing S II for the three sightlines under study are plotted in Figure 2, together with Voigt-profile fits to the data. These were conducted via simultaneous fits to unblended regions of the spectra, taking account of the COS line spread function, and leaving all the initial inputs (velocity centroid, line width, and column density) free to vary (following Lehner et al. 2011). Clear S II absorption from the SC is seen in each direction.

An important issue in abundance determinations is velocity alignment. The S II and H I lines should line up in velocity space if they originate in the same cloud. For PG 2112+059, weak 21 cm emission from the SC is visible in the range ~30–80 km s^{-1} (see Figure 2), matching the range where absorption is seen in S II; the fitted SC S II component has a centroid of 41.5 ± 14.5 km s^{-1}, with no evidence for misalignment from H I. For RX J2139.7+0246, the 21 cm component centroid (55 km s^{-1}) and S II component centroid (53.7 ± 5.3 km s^{-1}) are closely aligned. However, for RX J2043.1+0324, there is an ≈20 km s^{-1} offset between the S II component at 58.5 ± 6.1 km s^{-1} and the GBT H I component centered at 79 km s^{-1}. To explore this, we downloaded the Leiden–Argentine–Bonn (LAB) 21 cm data of this sightline (Kalberla et al. 2005), and found the SC emission in the LAB data was centered at 62 km s^{-1}, within the 1σ error of the S II centroid. The GBT data (9.′1 beam) have higher angular resolution than the LAB data (36′ beam) and have better sampling, but the fact that the GBT and LAB centroids disagree shows that small-scale structure (clumping) exists in the neutral gas in this direction. Indeed, we know there is a large gradient in N(H I) in this sightline since it passes just outside the main body of the SC (Figure 1). This structure limits the accuracy of abundances derived by comparing pencil-beam metal columns with finite-beam H I columns; we add a systematic error of ≈0.10 dex to the abundance calculations to account for this beam-size mismatch (Wakker et al. 2001).

The sulfur abundance in the SC is calculated from the observed S II ion abundance using an IC. The ion abundance is

Table 1
Properties of AGNs Behind the Smith Cloud

Target	l[a] (°)	b[a] (°)	z_{em}[b]	FUV[c]	F_{1300}[d] (flux units)	log N(H I)[e] (cm^{-2})	v_{min}[f] (km s^{-1})	v_{max}[f] (km s^{-1})	v_0[g] (km s^{-1})
PG 2112+059	57.04	−28.01	0.457	17.05	0.75	18.72 ± 0.06	40	75	42
RX J2043.1+0324	49.72	−22.88	0.271	17.29	0.55	18.84 ± 0.05	40	110	79
RX J2139.7+0246	58.09	−35.01	0.260	16.79	0.79	19.41 ± 0.02	40	100	55

Notes.
[a] Galactic longitude and latitude.
[b] Emission-line redshift of AGN.
[c] *GALEX* FUV magnitude.
[d] Spectroscopic flux at 1300 Å in units of 10^{-14} erg cm^{-2} s^{-1} Å^{-1}.
[e] H I column density in SC measured from GBT, integrated in range v_{min} to v_{max}, except for PG 2112+059 value, determined by profile fitting.
[f] Minimum and maximum LSR velocities of SC emission and absorption.
[g] Central LSR velocity of SC 21 cm emission.

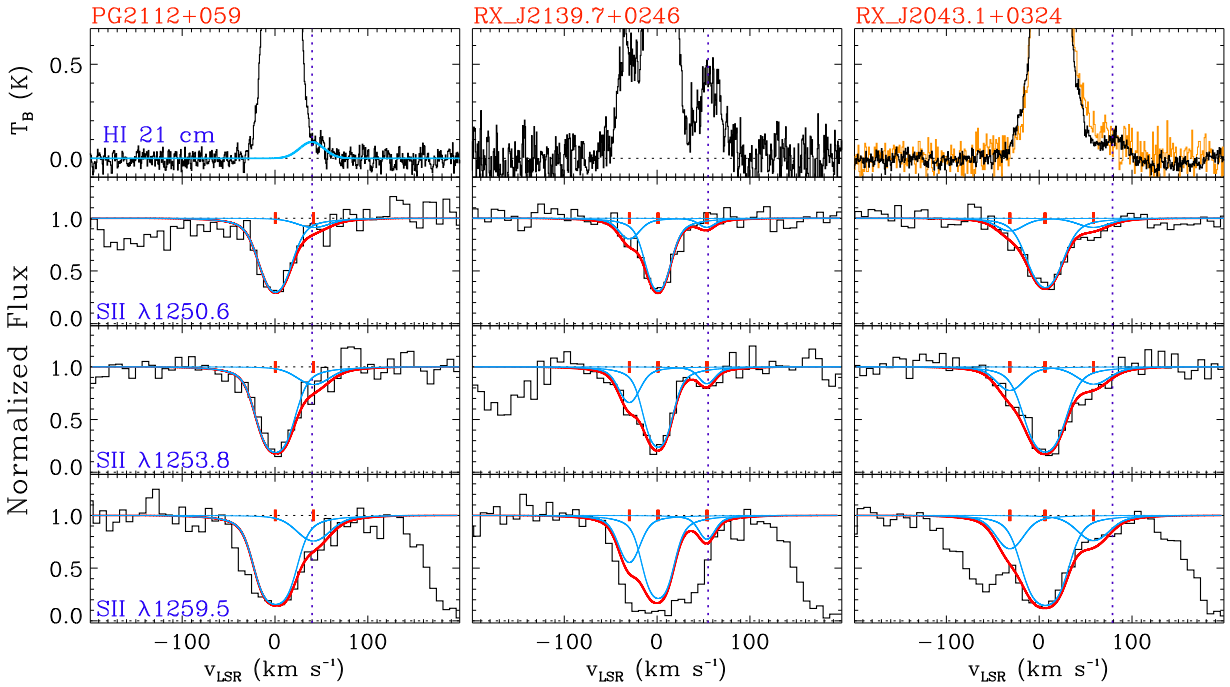

Figure 2. *HST*/COS S II λλ1250,1253,1259 absorption-line profiles of the three AGNs in our sample, together with GBT 21 cm H I emission profiles (top panels). In the case of RX J2043.1+0324, the LAB 21 cm data are shown in yellow. The red solid line shows Voigt-profile fits to the COS data, which are binned by three pixels for display. The fits are composed of two or three individual components, plotted as blue solid lines, with centroids denoted by tick marks. The positive-velocity component is due to the Smith Cloud; it covers the range ≈40–100 km s^{-1}. The dashed vertical line in each panel shows the central velocity of the SC in the GBT data. Good alignment between the S II absorption and GBT H I emission is seen in the first two sightlines, but there is a ≈20 km s^{-1} offset in the third sightline. This is likely related to small-scale structure in the GBT beam, which is already suggested by the difference between the LAB and GBT profiles.

determined observationally as:

$$[\mathrm{S\,II/H\,I}] = [\log N(\mathrm{S\,II}) - \log N(\mathrm{H\,I})] - \log(\mathrm{S/H})_{\odot} \quad (2)$$

and the IC is defined such that

$$[\mathrm{S/H}] = [\mathrm{S\,II/H\,I}] + \mathrm{IC(S)}. \quad (3)$$

The magnitude of the IC in a given direction depends on the H I column density, the ionization parameter $U \equiv n_{\gamma}/n_{\mathrm{H}}$ (the ratio of the ionizing photon density to the gas density), and the shape and normalization of the incident ionizing radiation field. We ran a grid of *Cloudy* photoionization models (Ferland et al. 2013) to investigate the magnitude of the ICs in the SC given a 3D model of the Galactic ionizing radiation field (Bland-Hawthorn & Maloney 1999; Fox et al. 2005, 2014), as a function of N(H I) and U (see Figure 3). These models use the radiation field interpolated at the location where each sightline intercepts the SC (given that we know l, b, and d). This field has $\log n_{\gamma} = -4.70$, corresponding to an ionizing flux $\Phi = 10^{5.78}$ photons cm^{-2} s^{-1}. We constrain the value of U by matching the Si III/Si II column-density ratio in the SC, $\log[N(\mathrm{Si\,III}\ 1206)/N(\mathrm{Si\,II}\ 1304)] \gtrsim -0.89$ in the RX J2043.1+0324 direction and $\gtrsim -0.99$ in the RX J2139.7+0246 direction, as measured from apparent optical depth (AOD) integrations (Savage & Sembach 1991) in the SC velocity interval. This process gives $\log U = -3.2 \pm 0.1$ and -3.0 ± 0.1, respectively, for these two sightlines (in line with values derived for other HVCs; Collins et al. 2005; Tripp & Song 2012; Fox et al. 2014). The IC for sulfur is then calculated directly for each sightline (via Equation (3)) using the model run at the appropriate N(H I) and U. Any hidden saturation in Si III 1206 (or Si II 1304) would raise (or lower) the

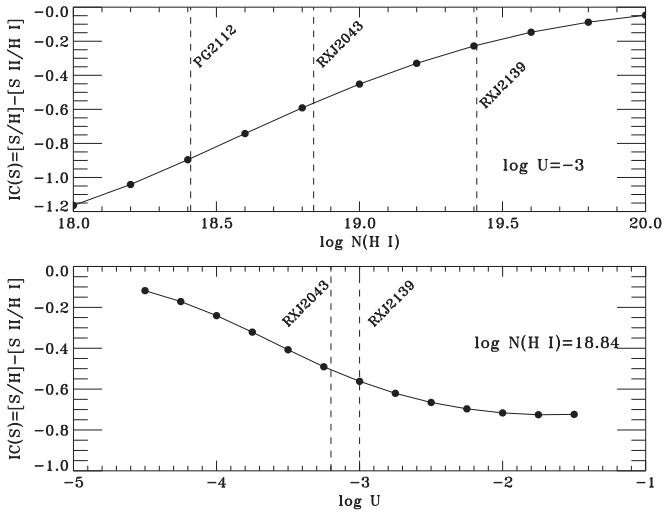

Figure 3. Ionization correction IC(S) as a function of H I column density (top) and ionization parameter (bottom), used to convert the measured [S II/H I] ratios to [S/H] abundances. The ICs were calculated using *Cloudy* photoionization models and a Galactic ionizing radiation field calculated at the position $l = 45°$, $b = -20$ °, $d = 12.5$ kpc, which has an ionizing photon density $\log(n_\gamma/\mathrm{cm}^{-3}) = -4.70$ (Fox et al. 2014). In the top panel, the ICs were calculated at $\log U = -3.0$, the value required to match the observed Si III/Si II ratio in the Smith Cloud, and the observed H I column densities in the three sightlines are shown with vertical lines. In the bottom panel, the ICs were calculated at a $\log N(\mathrm{H\,I}) = 18.84$, appropriate for the RX J2043.1+0324 sightline.

Si III/Si II ratio and push the solution for U to slightly higher (or lower) values. However, because the IC is insensitive to U, particularly at $\log U \gtrsim -3$ (see Figure 3, lower panel), this would not significantly change the IC.

The sulfur abundance measurements calculated using Equations (2) and (3) are summarized in Table 2. Among our three SC sightlines, the RX J2139.7+0246 direction has a high enough H I column density in the SC, $\log N(\mathrm{H\,I}) = 19.41$, that the IC is relatively small (−0.22 dex), giving [S/H] $= -0.56 \pm 0.20(\mathrm{stat}) \pm 0.15(\mathrm{syst})$, where the statistical uncertainty reflects the measurement error on the S II column density, and the systematic uncertainty derives from the UV–radio beam-size mismatch and the uncertainties in the IC. Toward PG 2112+059 and RX J2043.1+0324, the ICs are larger (−0.65 and −0.56 dex, respectively) because of lower H I columns, giving [S/H] $= -0.09 \pm 0.33(\mathrm{stat}) \pm 0.15(\mathrm{syst})$ and [S/H] $= -0.14 \pm 0.13(\mathrm{stat}) \pm 0.15(\mathrm{syst})$ in these two directions. If there is no variation in the true metallicity across the cloud, a weighted mean of the three measurements can be used, giving [S/H] $= -0.28 \pm 0.14$ (equivalent to $0.53^{+0.21}_{-0.15}$ solar). However, the variation in abundance across the SC may be real. Indeed, the direction with the lowest derived abundance (toward RX J2139.7+0246, where [S/H] is ≈0.5 dex lower than in the other two sightlines) is the sightline farthest into the SC wake, where more metal mixing with the surrounding gas is expected to occur (Gritton et al. 2014). Thus we see tentative evidence for an abundance gradient.

For comparison, the N abundance in the $\sim 10^4$ K ionized gas in the leading edge of the SC is 0.15–0.44 solar, as derived from optical [N II] emission lines and assuming the ionized gas is photoionized (although shocks may play a role there; Hill et al. 2009, 2013). In a downstream portion of the cloud, more analogous to the sightlines probed in this work, the derived N abundance is 0.3–0.8 solar (Putman et al. 2003; Hill et al. 2013). These results suggest that the SC has a solar or sub-solar N/α ratio.

4. DISCUSSION AND SUMMARY

The SC directly addresses a question of broad general interest: how does gas get into galaxies? Since the SC is a coherent H I cloud that has survived to its current location without breaking apart, it clearly exemplifies one pathway to bring fuel into galaxies. This begs the question: what is the origin of that pathway?

Our measurement of high metallicity ($0.53^{+0.21}_{-0.15}$ solar) argues in favor of a Galactic origin for the SC, such as gas on the returning leg of a fountain (Bregman 1980) launched into the halo at a different location in the disk (Sofue et al. 2004). Given the Galactic radial chemical abundance gradient of -0.06 dex kpc^{-1} (Henry & Worthey 1999), half-solar metallicity is reached at a Galactocentric radius of 13 kpc, which is exactly where the last SC disk passage occurred in the Lockman et al. (2008) trajectory. Therefore the metallicity and orbit of the SC are both consistent with an origin in the outer disk.

If the SC were accreting for the first time from the IGM, or is the remnant ISM of a dwarf galaxy (Bland-Hawthorn et al. 1998), it would have a lower metallicity. The LMC has ≈0.50 solar metallicity, but is orders of magnitude more massive than the SC, and all other Local Group dwarfs have lower metallicity. Stark et al. (2015) noted how the newly discovered star-forming galaxy Leo P has similar properties to the SC, and would also not show stars if at the SC's location. However, Leo P has a metallicity of 3% solar (Skillman et al. 2013). Our SC metallicity conclusively rules out such a galaxy as the cloud's origin.

Our abundance calculations have not taken into account the depletion of sulfur onto dust grains (Jenkins 2009). However, any such depletion would *raise* the total (gas+dust) inferred sulfur abundance, strengthening the conclusion that the SC is Galactic. Furthermore, if any metal mixing has occurred in the Cloud's past, so that it represents a diluted mixture of Galactic and extragalactic material, the fact that the resulting metallicity is as high as ≈half solar again strengthens the conclusion that Galactic (enriched) gas contributed to its origin (see Bland-Hawthorn et al. 2015 and Webster et al. 2015 for recent arguments concerning metal mixing).

It has long been a mystery how the SC survived to reach its current location, because infalling HVCs are predicted and observed to be disrupted by their interaction with the surrounding gaseous medium. The lifetime against disruption depends on the cloud's mass (Heitsch & Putman 2009) and density contrast with the external medium (Joung et al. 2012). One possibility, explored by Nichols & Bland-Hawthorn (2009) and Galyardt & Shelton (2015), is that the SC might be a dark galaxy, bearing dark matter and gas but no stars. The dark matter would provide the confinement that allowed the cloud to survive the ≈70 Myr since its last disk passage. Our detection of metals argues against this idea, since the metals require star formation to have occurred.

Another possibility to consider is whether the SC is a dark matter halo that accreted sufficient disk material on a previous passage to explain its high metallicity. Using the disk column of Nichols et al. (2014) and the cloud's trajectory, the SC would travel through an ISM mass of $M_{\mathrm{ISM}} \approx 2.3 \times 10^5 (R_{\mathrm{SC}}/100\ \mathrm{pc})^2\ M_\odot$ during a single pass

Table 2
Smith Cloud Metallicity Measurements

Target	log N(H I)	log N(S II)[a]	[S II/H I][b]	log $\frac{N(\mathrm{Si\ III})}{N(\mathrm{Si\ II})}$[c]	log U[d]	IC(S)[e]	[S/H][f]
PG 2112+059	18.72 ± 0.06	14.40 ± 0.33	+0.56 ± 0.33	...[g]	≈ -3.0	−0.65 ± 0.10	−0.09 ± 0.33 ± 0.15
RX J2043.1+0324[h]	18.84 ± 0.05	14.38 ± 0.13	+0.42 ± 0.13	$\gtrsim -0.89$	−3.2 ± 0.1	−0.56 ± 0.10	−0.14 ± 0.13 ± 0.15
RX J2139.7+0246	19.41 ± 0.02	14.17 ± 0.20	−0.36 ± 0.20	$\gtrsim -0.99$	−3.0 ± 0.1	−0.22 ± 0.10	−0.58 ± 0.20 ± 0.15

Notes. We use the solar sulfur abundance log $(\mathrm{S/H})_\odot = -4.88$ from Asplund et al. (2009).
[a] Column density derived from Voigt-profile fitting (see Figure 2).
[b] S II ion abundance, defined in Equation (2).
[c] Si III/Si II column-density ratio, measured in the velocity interval $v_{\rm min}$ to $v_{\rm max}$.
[d] Logarithm of best-fit ionization parameter, derived to match the Si III/Si II ratio.
[e] Ionization correction derived from *Cloudy* photoionization models (Figure 3).
[f] S abundance corrected for ionization, [S/H] = [S II/H I] + IC(S). The first error is statistical. The second is systematic and accounts for the beam-size mismatch between UV and radio observations, and uncertainties in the ICs.
[g] Contamination prevents the Si III/Si II ratio from being measured; we adopt the same log U value as derived for the RX J2139.7+0246 sightline.
[h] This sightline shows a ≈20 km s^{-1} offset between the S II and GBT H I centroids (see Figure 2).

through the disk, which is ≈10% of the SC mass for a projected radius $R_{\rm SC} = 100$ pc. However, this assumes that the cloud incorporates *all* of the gas mass it travels through, which is unrealistic. Simulations show that the accretion efficiencies are ≈0.1%–1%, depending on the time and velocity (F. Heitsch et al. 2016, in preparation), making it challenging for this scenario to explain our metallicity observations.

Although our sulfur abundance is supportive of a Galactic origin for the SC, there remain two main hurdles for this hypothesis: the cloud's mass and kinematics. The mass problem is that the SC's high mass ($\approx 2 \times 10^6 M_\odot$) is much larger than that of known extraplanar Galactic H I clouds, such as superbubble "caps," and makes it unlikely that any star-formation process in the disk is energetic enough to explain the SC (Hill et al. 2009). For example, the cap to the Ophiuchus superbubble contains only $\approx 3 \times 10^4 M_\odot$ of H I (Pidopryhora et al. 2007). However, recent theoretical work on Galactic fountains has shown they can sweep up and cool coronal gas (Marinacci et al. 2010; Marasco et al. 2013). In such models the mass of fountain HVCs grows with time as they accrete cooled coronal material. In the hydrodynamical simulations of Fraternali et al. (2015), an HVC can increase its mass by a factor of three in 200 Myr. The mass problem would be alleviated by such a mechanism, because then the current SC mass would be higher than its launch mass and so the required launch energy would be lower than previously thought.

The second problem is the SC's kinematics. There is direct evidence in the GBT H I data that the Cloud has a line of sight velocity at least 70 km s^{-1} greater than the Galactic halo material it is encountering (Lockman et al. 2008). The SC orbit is prograde and inclined at a shallow angle relative to the Milky Way disk (≈30°). This indicates that the cloud is moving faster than Galactic rotation, and such super-rotation is not commonly observed: in other galaxies a *lag* in rotation of gaseous material thrown up above the plane is typically seen (Boomsma et al. 2005; Sancisi et al. 2008). A super-rotating extraplanar cloud would be unique.

In conclusion, our sulfur abundance of $0.53^{+0.21}_{-0.15}$ solar for the SC provides an important new clue on its origin and supports a Galactic (as opposed to extragalactic) explanation, effectively ruling out dwarf-galaxy and dark-galaxy origins. However, the cloud's mass and kinematics require it to be a highly unusual Galactic cloud. This enigmatic object is still to be fully explained.

The authors are grateful to Robin Shelton, Ken Croswell, and the referee for valuable comments. Support for program 13840 was provided by NASA through grants from the Space Telescope Science Institute, which is operated by the Association of Universities for Research in Astronomy, Inc., under NASA contract NAS 5-26555.

REFERENCES

Asplund, M., Greenness, N., Jacques Sauval, A., & Scott, P. 2009, ARA&A, 47, 481
Bland-Hawthorn, J., & Maloney, P. R. 1999, ApJL, 510, L33
Bland-Hawthorn, J., Sutherland, R., & Webster, D. 2015, ApJ, 807, 154
Bland-Hawthorn, J., Veilleux, S., Cecil, G. N., et al. 1998, MNRAS, 299, 611
Boomsma, R., Oosterloo, T. A., Fraternali, F., van der Hulst, J. M., & Sancisi, R. 2005, A&A, 431, 65
Boothroyd, A. I., Blagrave, K., Lockman, F. J., et al. 2011, A&A, 536, A81
Bregman, J. 1980, ApJ, 236, 577
Collins, J. A., Shull, J. M., & Giroux, M. L. 2005, ApJ, 623, 196
Ferland, G. J., Porter, R. L., van Hoof, P. A. M., et al. 2013, RMxAA, 49, 137
Fox, A. J., Wakker, B. P., Barger, K. A., et al. 2014, ApJ, 787, 147
Fox, A. J., Wakker, B. P., Savage, B. D., et al. 2005, ApJ, 630, 332
Fraternali, F., Marasco, A., Armilotta, L., & Marinacci, F. 2015, MNRAS, 447, L70
Galyardt, J., & Shelton, R. L. 2015, arXiv:1511.05884
Green, J. C., Froning, C. S., Osterman, S., et al. 2012, ApJ, 744, 60
Gritton, J. A., Shelton, R. L., & Kyujin, K. 2014, ApJ, 795, 99
Heitsch, F., & Putman, M. E. 2009, ApJ, 698, 1485
Henry, R. B. C., & Worthey, G. 1999, PASP, 111, 919
Hill, A. S., Haffner, L. M., & Reynolds, R. J. 2009, ApJ, 703, 1832
Hill, A. S., Mao, S. A., Benjamin, R. A., Lockman, F. J., & McClure-Griffiths, N. M. 2013, ApJ, 777, 55
Jenkins, E. B. 2009, ApJ, 700, 1299
Joung, M. R., Bryan, G. L., & Putman, M. E. 2012, ApJ, 745, 148
Kalberla, P. M. W., Burton, W. B., Hartmann, D., et al. 2005, A&A, 440, 775
Lehner, N., & Howk, J. C. 2011, Sci., 334, 955
Lehner, N., Zech, W. F., Howk, J. C., & Savage, B. D. 2011, ApJ, 727, 46
Lockman, F. J. 2015, in Proc. IAU Symp. 315 (Cambridge: Cambridge Univ. Press), in press (arXiv:1511.05423)
Lockman, F. J., Benjamin, R. A., Heroux, A. J., & Langston, G. I. 2008, ApJL, 679, L21
Marasco, A., Marinacci, F., & Fraternali, F. 2013, MNRAS, 433, 1634
Marinacci, F., Binney, J., Fraternali, F., et al. 2010, MNRAS, 404, 1464
Nichols, M., & Bland-Hawthorn, J. 2009, ApJ, 707, 1642
Nichols, M., Mirabel, N., Agertz, O., Lockman, F. J., & Bland-Hawthorn, J. 2014, MNRAS, 442, 2883
Pidopryhora, Y., Lockman, F. J., & Shields, J. C. 2007, ApJ, 656, 928
Putman, M. E., Bland-Hawthorn, J., Veilleux, S., et al. 2003, ApJ, 597, 948
Putman, M. E., Peek, J. E. G., & Joung, M. R. 2012, ARA&A, 50, 491
Sancisi, R., Fraternali, F., Oosterloo, T., & van der Hulst, T. 2008, A&ARv, 15, 189
Savage, B. D., & Sembach, K. R. 1991, ApJ, 379, 245

Shull, J. M., Jones, J. R., Danforth, C. W., & Collins, J. A. 2009, ApJ, 699, 754
Skillman, E. D., Salzer, J. J., Berg, D. A., et al. 2013, AJ, 146, 3
Smith, G. P. 1963, BAN, 17, 203
Sofue, Y., Kudoh, T., Kawamura, A., Kazunari, S., & Fujimoto, M. 2004, PASJ, 56, 633
Spitoni, E., Recchi, S., & Matteucci, F. 2008, A&A, 484, 743
Stark, D. V., Baker, A. D., & Kannappan, S. J. 2015, MNRAS, 446, 1855
Tripp, T. M., & Song, L. 2012, ApJ, 746, 173
Wakker, B. P., Hernandez, A. K., French, D., et al. 2015, ApJ, 814, 40
Wakker, B. P., Kalberla, P. M. W., van Woerden, H., de Boer, K. S., & Putman, M. E. 2001, ApJS, 136, 537
Wakker, B. P., & van Woerden, H. 1997, ARA&A, 35, 217
Wakker, B. P., York, D. G., Wilhelm, R., et al. 2008, ApJS, 146, 1
Webster, D., Frebel, A., & Bland-Hawthorn, J. 2015, ApJ, submitted (arXiv:1509.00856)